TBP: Temporal Beam Prediction for Mobile Millimeter-Wave Networks

Shichen Zhang, Qiben Yan, *Senior Member, IEEE,* Tianxing Li, Li Xiao, *Senior Member, IEEE,* and Huacheng Zeng, *Senior Member, IEEE*

***Abstract*—Beam selection is a fundamental problem in millimeter wave (mmWave) communication systems. Yet, most existing beam selection techniques focus on the exploitation of spatial channel features to reduce their airtime overhead in stationary mmWave networks. In this paper, we exploit the *temporal correlation* of wireless channels to facilitate beam selection in mobile mmWave networks. Specifically, we present a Temporal Beam Prediction (TBP) scheme for a mobile mmWave device to predict its future beam direction based on its history beam selection profile. TBP has two challenges in its design: i) non-uniform history data samples due to the bursty nature of data traffic; and ii) non-smooth beam angles over time due to the multipath effect of channels and the imperfect radiation pattern of phased-array antennas. TBP addresses these two challenges by employing a new mobility-aware LSTM model that takes data timestamp for its training, together with an adversarial learning model to exploit user-independent features for beam steering. We have evaluated TBP through over-the-air (OTA) experiments on a 60 GHz mmWave testbed. Experimental results show that the average prediction error of TBP is less than 7 degrees and that TBP improves the throughput by 60% in representative mmWave networks.**

***Index Terms*—wireless networks, mmWave communications, beamforming, deep learning**

I. Introduction

Millimeter wave (mmWave) will be the bedrock for 5G and beyond wireless networks to realize the vision of smart society and digitized physical world by offering ultra-low latency, multi-Gbps, scalable wireless connections for emerging applications such as virtual reality (VR), cloud-centric real-time AI, and high-resolution video streaming [1]. In mmWave networks, devices are reliant on analog beamforming to combat high path loss. In practice, a set of beam angles are predefined, and the analog beamforming operation for a mmWave device is equivalent to the selection of the best beam index that can maximize the signal strength at a receiver. If candidate beams are probed sequentially and exhaustively to identify the best one, the beam search process will entail a large airtime overhead. The emerging applications such as augmented reality (AR) and virtual reality (VR) services have a high demand for bandwidth and communication latency. Therefore, it is critical to develop more efficient beam selection schemes that can reduce the beamforming overhead for mmWave devices.

S. Zhang, Q. Yan, T. Li, L. Xiao, and H. Zeng are with the Department of Computer Science and Engineering, Michigan State University, East Lansing, MI 48824 USA. (e-mail: sczhang@msu.edu; qyan@msu.edu; litianx2@msu.edu; lxiao@cse.msu.edu; hzeng@msu.edu). The corresponding author is H. Zeng (e-mail: hzeng@msu.edu). This work was supported in part by NSF Grants CNS-2100112 and CNS-2312448.

To reduce the airtime overhead of beam selection, different approaches have been studied for the management of beam search, such as out-of-band CSI-assisted beam selection [2], [3], [4], [5], compressive sensing [6], [7], [8], hierarchy beam search [9], [10], [11], [12], and learning-based beam search [13], [14], [15], [16], [17], [18]. These approaches have demonstrated a great success in the acceleration of beam selection and the reduction of its airtime overhead. However, most of prior efforts focus on the beam search optimization in a snapshot of networks by exploiting *spatial* features of mmWave channels. The exploitation of *temporal correlation* of mmWave channels for beam selection remains limited.

In this paper, we exploit temporal channel correlation of a mobile mmWave device to predict its future beam direction based on its history beam selection profile, with the aim of reducing the airtime overhead of beam search in mobile mmWave networks. Specifically, we present a Temporal Beam Prediction (TBP) scheme for a mobile mmWave device to estimate its future beam direction based on its history beam selection profile. TBP was motivated by the recent success of pedestrian trajectory prediction [19], [20], [21], for which recurrent neural network (RNN) models have demonstrated a great potential for accurate prediction. TBP borrows the idea from pedestrian trajectory prediction by using LSTM [22] as the model for beam prediction in mobile mmWave networks. LSTM has proved its efficiency and effectiveness in capturing the dynamic pattern of beam directions by retaining information about past directions. The internal memory can encapsulate details pertaining to the environment and user mobility, thereby achieving accurate prediction of the future beam direction. Specifically, TBP asks each mmWave device to record its beam angles adopted by its past packets, and uses its past beam angle profile to predict the best beam angles for its current or next packet transmission. As expected, the predicted beam angle might not be the best. So a beam refinement algorithm is employed to find the best one through a local search.

Compared to trajectory prediction, beam prediction has two new challenges. First, the past data samples (history beam selection results) are non-uniform over time due to the bursty nature of data traffic. For example, the time interval of VoIP traffic ranges from 5 ms to 40 ms [23], depending on the voice intensity. The non-uniformity of data samples calls for a new LSTM model that can take into account data timestamp for the beam angle prediction. Second, unlike movement trajectory, the best-beam angle trajectory may have sharp changes due to the multipath effect of wireless channels and the imperfect

radiation pattern of phased-array antennas. Consequentially, the best-beam angle trajectory is typically non-smooth over time, making it challenging to perform an accurate prediction.

To address these two challenges, TBP proposes a mobility-aware LSTM (mLSTM) model for the beam angle prediction. The novelty of mLSTM lies in a new structure of its cells, which takes both data samples (history beam angles) and their timestamps as the input to predict future beam angles. This is in sharp contrast to traditional LSTM, which does not consider the timestamps. The inclusion of data timestamps makes it possible for the mLSTM model to extract the time-dependent features, which is critical for improving the beam prediction accuracy. In addition, TBP employs an adversarial learning structure to extract the user-independent features for the beam prediction. The combination of CNN-based feature extractor, mLSTM-based beam angle predictor, and adversarial-learning discriminator appears to be an efficient model for the temporal beam prediction in mobile mmWave networks.

In addition, a wireless device may be equipped with both mmWave and sub-6GHz radios for its communications. For such a case, we enhance the design of TBP by leveraging the out-of-band channel state information (CSI) from co-located sub-6GHz radio to improve the accuracy of mmWave beam prediction. The key challenge here stems from the heterogeneity of data samples from the two radios. Specifically, mmWave radio generates beam indices (i.e., beam angles), while sub-6GHz radio generates channel coefficients (or channel matrix). Per our experiments, simple concatenation of data samples from the two radios as the input for beam prediction yields an inferior performance. To address this challenge, TBP converts sub-6GHz CSI to the corresponding beam angles by exploiting their inherent spatial relations. The converted beam angles will then be combined with mmWave beam angles for training and inference. Such a CSI-assisted learning model is particularly useful for cases where a mmWave radio does not have sufficient data samples for prediction (e.g., when a mmWave radio just wakes up from sleep mode).

We have built a prototype of TBP on a software-defined radio (SDR) 60GHz mmWave testbed. The mmWave device is equipped with a planar antenna with 4×8 patch antenna elements, and installed on a building's ceiling. We evaluated the performance of TBP in four scenarios: lab, conference room, hallway and apartment. Experimental measurement shows that the average prediction error of TBP is less than 7 degrees for both beam azimuth and elevation angles in most of our studied cases. Experimental measurement also shows that the utilization of out-of-band CSI can further improve the beam prediction accuracy for a mmWave device. Based on the measurement results, we simulate the throughput gain of TBP in a mobile mmWave network with representative traffic settings. The simulation results show that TBP can improve the throughput by more than 60% compared to existing approaches in all four scenarios.

The contributions for this paper are summarized as follows.

- To the best of our knowledge, TBP is the first system-focused beam prediction scheme that exploits the *temporal* correlation of mmWave channels along a device's movement trajectory to reduce the airtime overhead of beam search.
- TBP proposes a deep-learning network structure with new LSTM cells, which is capable of accommodating non-uniform, non-smooth data samples for accurate prediction. It also leverages out-of-band CSI to improve the beam prediction accuracy.
- TBP has been evaluated on a 60GHz mmWave testbed. Extensive experimental measurement confirms its effectiveness of beam prediction.

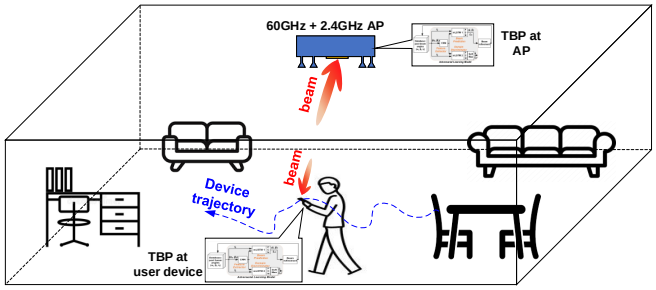

Fig. 1: Illustration of temporal beam prediction (TBP) for both mmWave AP and station (user device).

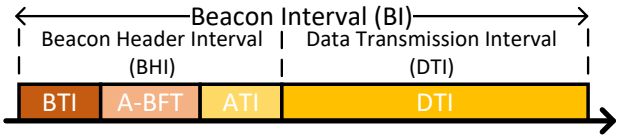

Fig. 2: The structure of beacon interval (BI) in 802.11ad.

II. Problem Description

We consider a mmWave communication network as shown in Fig. 1, where an access point (AP) is installed on the ceiling of a building to serve a set of stationary or mobile stations (user devices). To combat the high path loss, analog beamforming is adopted at both AP and station sides for signal energy steering. In practice, a set of beam angles are typically predefined for selection. As such, analog beamforming is equivalent to the selection of the best azimuth and elevation beam angles for a mobile device's phased-array antenna. In what follows, we first briefly introduce the beam search approaches in 802.11ad and 5G NR, and then present our design objective.

A. Preliminaries

Beam Search in IEEE 802.11ad/ay. IEEE 802.11ad [24] is a 60GHz mmWave communication standard. The beamforming training in 802.11ad comprises two phases: i) Sector Level Sweep (SLS), and ii) Beam Refinement Protocol (BRP). Fig. 2 shows the beacon interval (BI) structure in 802.11ad. The SLS takes place in the beacon header interval (BHI), while the BRP takes place in the data transmission interval (DTI). In the SLS phase, the user device configures its antenna to an omnidirectional radiation pattern, while the AP sweeps its beam over all possible directions. At the end of this process, the user device identifies the AP's best beam index

and reports it to the AP. After identifying the AP's best beam index, a similar operation is performed on the user side to find its best beam index. More specifically, the AP uses its identified best beam index, and the user device sweeps its beam over all possible directions. In the end, the AP will find the user device's best beam index and send it to the user. SLS is mandatory in IEEE 802.11ad, and its beam training process takes about 1.54 ms for 7-degree beamwidth [2]. While the SLS phase is mandatory, the BRP phase is optional in 802.11ad. In this phase, the beam selected from SLS is refined through an iterative procedure. While the goal of SLS is to establish the connection between two devices at the control mode rate, the goal of BRP is to optimize devices' antenna settings by making use of the TRN field in a frame. It allows for multiple measurements in the same packet and thus enables coherent measurements, leading to a significant performance improvement compared to SLS.

Compared to 802.11ad, 802.11ay introduces various enhancements and new concepts that improve beam training and extend its support for new applications. Some of the training-related enhancements are highlighted as follows: i) a new beamforming procedure, called BRP Transmit Sector Sweep (TXSS), was introduced to improve the efficiency of beamforming; ii) first path beamforming training is defined to support positioning applications; iii) group beamforming is specified to reduce overhead by enabling the training for multiple stations simultaneously; and iv) a new BRP packet called EDMG BRP-RX/TX packet is defined to enable concurrent Tx and Rx beam training.

Beamforming in 5G mmWave Networks. MmWave communication (on 24–47 GHz) is a key component of 5G New Radio (NR) in order to increase the network throughput. The beam training procedure in 5G is similar to that in 802.11ad. The base station initiates the beam search process by sweeping its beam over all possible directions. At the end of this period, the user equipment identifies the best beam index for the base station and reports it to the base station. This process repeats with a smaller beamwidth at the base station, until the base station obtains its best beam index. After that, the base station fixes the beam direction and the user equipment sweeps over its beam angles to find the best one.

B. Design Objective

The airtime overhead of beam training in both 802.11ad/ay and 5G NR is $\mathcal{O}(N)$, where N is the number of beam candidates. While many schemes (e.g., [7], [25], [3], [26], [27]) have been proposed to reduce the overhead, most of them are limited to the exploitation of spatial-domain channel features in a snapshot of the network. Inspired by the pedestrian trajectory prediction [19], [20], [21], this paper focuses on the system-perspective design of efficient beam search strategies for a mobile mmWave device by exploiting the *temporal channel correlation* over its movement trajectory, aiming to reduce the airtime overhead of its beam training procedure.

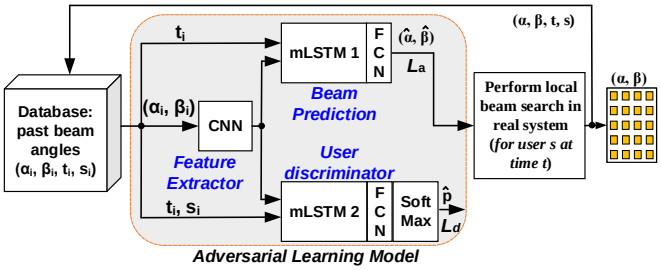

Fig. 3: The overview of TBP.

III. TBP: Design

A. Overview

Fig. 3 shows the system architecture of TBP for a mobile mmWave device to predict its future beam angles based on its past beam selection results. The system has a database to record the past beam information, i.e., $(\alpha_i, \beta_i, t_i, s_i)$, where i is the data sample (beam) index ($i = 1, 2, \cdots, N$), α_i is the beam azimuth beam angle, β_i is the elevation beam angle, t_i is the time moment when this data sample is generated, and s_i is the ID of the user device for whose data sample is generated. A CNN is used to extract the features of beam azimuth and elevation angles. Two mLSTM branches are adopted in the system. One is used for prediction, and the other is used as the user device discriminator for adversarial learning. The rationale behind this design is that we wish to extract the beam features that are independent of individual user devices, so that this design is generally applicable. The user device discriminator (i.e., mLSTM 2 in Fig. 3) is used for this purpose.

The predicted beam angles go through the *local* beam search procedure in real mmWave systems to find the optimal beam angles. The final selected beam is used by the antenna for signal steering and sent to the database for future use. The key components of TBP are highlighted as follows.

- *CNN for Feature Extraction:* As shown in Fig. 3, a CNN is used to extract features before sending data to the mLSTM modules. The CNN has 12 kernels with a size of 4, and it uses ReLU as the activation function.
  The kernel size and the number of kernels are adjusted based on the model's performance. Smaller kernel sizes excel at capturing fine-grained features, while larger ones are adept at capturing broader patterns. Given that TBP aims to capture dynamic patterns, the beam prediction is oriented towards the current moment; hence, larger kernel sizes might overlook the optimal beam direction at the present time. While a higher number of kernels enhances the feature space, it amplifies the model complexity. Based on our experimental observations, we employ 12 kernels to extract the features of the data. Besides, the causal padding is employed to avoid the time length changes.
- *mLSTM and Adversarial Learning:* Referring to Fig. 3, two identical mLSTM networks are used in TBP. These two mLSTM networks are structured for adversarial learning, following the architecture in [28]. The first

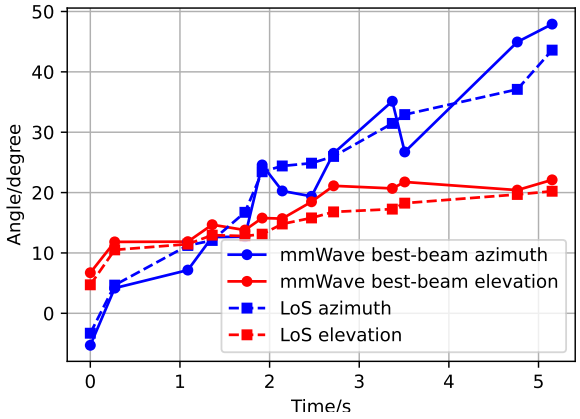

Fig. 4: Experimental data that show the comparison between a mmWave AP's best-beam direction and its LoS direction when communicating with a station.

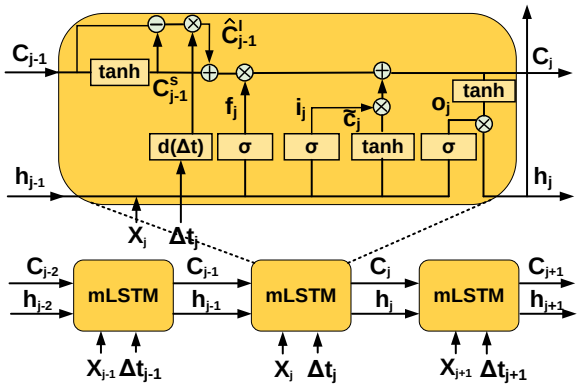

Fig. 5: The structure of the mLSTM.

mLSTM is for predicting the beam angles based on the history information, while the second mLSTM is used to predict the user device. We note that the training purpose is to enable the CNN to deceive the second mLSTM, thereby allowing the CNN to extract user-independent features. Both mLSTMs are connected to the fully connected layers. In addition, mLSTM 2 is added with a SoftMax layer after a fully-connected layer. The output of SoftMax is the possibilities of the devices by which the data samples are generated.

- *Local Beam Search in Real System:* Since the predicted beam may not be the best one, a local beam search module is employed to perform beam refinement in real systems. It follows the specified protocol, with the aim of finding the optimal beam for data transmission and therefore improving the efficiency of transmission. Details are given in Section III-D.

B. mLSTM: Mobility-Aware LSTM

The prediction of mmWave beam azimuth and elevation angles has two unique challenges: *non-uniform* and *non-smooth* data samples over time. Fig. 4 shows our experimental results of comparison between the best-beam direction and the LoS direction in a lab scenario. It can be seen that the time intervals of consecutive data samples are not identical. This is because data traffic is bursty in nature. It can also be seen that the best beam angles may differ from and less smooth than LoS angles over time. This is caused by the multipath effect and non-ideal antenna radiation. To address these challenges, we propose an LSTM model for a mobile device to predict its beam angles based on its past beam selection profile.

RNN has been widely used for processing time-series sequential data. Connections between hidden units form a cycle that can send the past memory to the current cell. In this way, RNNs are particularly useful for dealing with the problem where the past memory has a strong effect on the current status. However, RNNs is incapable of capturing long-term dependence because of the vanishing and exploding gradient problems [22]. LSTM, a special case class in RNN, can handle long-term memory without the problem mentioned above.

A traditional LSTM cell has four parts: forget gates, input gates, output gates, and a cell state. The input time-series data for the traditional LSTM cell is assumed uniformly distributed, disregarding the time intervals between samples. This means that the time gaps between consecutive samples are not taken into consideration during the data processing. However, the time series data is not always uniformly distributed especially when we consider communication requests. The communication frequency depends on the users' needs and also the type of data the user requested. The data from the mmWave band only obey the Poisson distribution.

Given the non-uniformity and non-smoothness of the beam angles over the device's movement trajectory, traditional LSTM models may not work well for the prediction (e.g., [29], [30]). This coincides with our experimental observations. To solve this problem, we propose a new mobility-aware LSTM (mLSTM) model for the beam prediction over time, as shown in Fig. 5. The input includes both data samples (past beam angles) and their timestamp. The output is the predicted beam angles at a given time moment. In this mLSTM structure, the memory from the previous time slot is first decomposed into short-term memory through a data-driven method. Unlike the time-aware LSTM in [31], which discounts on short-term memory, our mLSTM extracts the long-term memory and discounts on it. The intuition behind this operation is that, for the beam prediction problem, the short-term memory should carry higher weights for the prediction. In other words, the near-past beam samples should play a more important role in the prediction than the far-past beam samples. Still, the long-term memory is kept to capture the general moving tendency. Comparing with the traditional LSTM, the memory is adjusted with a larger amount of short-term memory and a fewer long-term memory. To discount the long-term memory, mLSTM utilizes a non-increasing function on the time interval and multiplies it with the long-term memory.

Fig. 5 shows the diagram of our proposed mLSTM, where each of its cells can be mathematically expressed as follows:

$$\mathbf{c}^{\mathrm{s}}_{j-1} = \tanh(\mathbf{W}_s \mathbf{c}_{j-1} + \mathbf{b}_s) \tag{1a}$$

$$\mathbf{c}^{\mathrm{l}}_{j-1} = \mathbf{c}_{j-1} - \mathbf{c}^{\mathrm{s}}_{j-1} \tag{1b}$$

$$\Delta t_j = t_j - t_{j-1} \tag{1c}$$
$$\hat{\mathbf{c}}^{\mathrm{l}}_{j-1} = \mathbf{c}^{\mathrm{l}}_{j-1} \odot d(\Delta t_j) \tag{1d}$$
$$\hat{\mathbf{c}}_{j-1} = \hat{\mathbf{c}}^{\mathrm{l}}_{j-1} + \mathbf{c}^{\mathrm{s}}_{j-1} \tag{1e}$$
$$\mathbf{i}_j = \sigma(\mathbf{W}_{xi}\mathbf{x}_j + \mathbf{W}_{hi}\mathbf{h}_{j-1} + \mathbf{b}_i) \tag{1f}$$
$$\mathbf{f}_j = \sigma(\mathbf{W}_{xf}\mathbf{x}_j + \mathbf{W}_{hf}\mathbf{h}_{j-1} + \mathbf{b}_f) \tag{1g}$$
$$\mathbf{o}_j = \sigma(\mathbf{W}_{xo}\mathbf{x}_j + \mathbf{W}_{ho}\mathbf{h}_{j-1} + \mathbf{b}_o) \tag{1h}$$
$$\tilde{\mathbf{c}}_j = \tanh(\mathbf{W}_{xc}\mathbf{x}_j + \mathbf{W}_{hc}\mathbf{h}_{j-1} + \mathbf{b}_c) \tag{1i}$$
$$\mathbf{c}_j = \mathbf{f}_j \odot \hat{c}_{j-1} + \mathbf{i}_j \odot \tilde{\mathbf{c}}_j \tag{1j}$$
$$\mathbf{h}_j = \mathbf{o}_j \odot \tanh(\mathbf{c}_j), \tag{1k}$$

where $\mathbf{x}_j$ is the input data, Δt_j is the relative timestamp calculated from the database, $\mathbf{h}_{j-1}$ is the previous hidden state, and $\mathbf{c}_{j-1}$ is the previous memory. $\mathbf{W}_{xi}, \mathbf{W}_{hi}, \mathbf{b}_i$ are the parameters for input gate. $\mathbf{W}_{xf}, \mathbf{W}_{hf}, \mathbf{b}_f$ are the parameters for forget gate. $\mathbf{W}_{xo}, \mathbf{W}_{ho}, \mathbf{b}_o$ are the parameters for output gate. $\mathbf{W}_{xc}, \mathbf{W}_{hc}, \mathbf{b}_c$ are the parameters for candidate memory. $\mathbf{c}^{\mathrm{s}}_{j-1}$ is the short-term memory, which is decomposed from previous memory cell $\mathbf{c}_{j-1}$; $\mathbf{W}_s$ and $\mathbf{b}_s$ are new weight matrix and bias vector defined for this operation, respectively. $\mathbf{c}^{\mathrm{l}}_{j-1}$ is the long-term memory, and $\hat{\mathbf{c}}^{\mathrm{l}}_{j-1}$ is the discounted long-term memory. Here, the non-increasing function being used is $d(\Delta t) = 1/\Delta t$. $\hat{\mathbf{c}}_{j-1}$ is the final adjusted memory which includes the full short-term memory and the discounted long-term memory. It is used to update the memory. This mLSTM is the fundamental building block for the design of TBP.

C. Automated Training Process

Data collection Automation. A mmWave device first works in the traditional beam training mode (e.g., using 802.11ad or 5G NR beam training protocol [32], [33]) to collect data samples for the training of TBP. A data sample can be denoted as $(\alpha_i, \beta_i, t_i, s_i)$, where i is the sample index. After sufficient data samples have been collected, TBP starts to train its models. As shown in Fig. 3, after TBP completes its model training and enters its inference phase, it will still add data samples to its database, which can be further used to train its model if necessary. It should be noted that the training process will not disrupt the normal communications of a mmWave device, as the data samples are side information from standard-compatible mmWave communication.

Training of TBP. Following the structure in Fig. 3, mLSTM 1 is trained to minimize the following loss function: $\mathcal{L}_{\mathrm{a}} = \frac{1}{N}\sum_{i=1}^{N}[(\hat{\alpha}_i - \alpha_i)^2 + (\hat{\beta}_i - \beta_i)^2]$, where (α_i, β_i) are the beam angles of a data sample, $(\hat{\alpha}_i, \hat{\beta}_i)$ are the prediction results (see Fig. 3), and N is the total number of training samples in this mini-batch. Denote $\mathbf{W}_{\mathrm{a}}$ as the weights of mLSTM 1. Then, they are updated as follows: $\mathbf{W}_{\mathrm{a}} \leftarrow \mathbf{W}_{\mathrm{a}} - \mu_{\mathrm{a}}\frac{\partial \mathcal{L}_{\mathrm{a}}}{\partial \mathbf{W}_{\mathrm{a}}}$, where μ_{a} is the update step size ($\mu_{\mathrm{a}} = 0.01$ in our experiments).

mLSTM 2 serves as a user device discriminator. It shares the identical structure of mLSTM 1. Denote $\vec{p}_i$ as the output probability vector of the SoftMax layer when the input data sample is $(\alpha_i, \beta_i, t_i, s_i)$. We define its loss function as: $\mathcal{L}_{\mathrm{d}} = -\frac{1}{N}\sum_{i=1}^{N}\log(g(\vec{p}_i, s_i))$, where $g(\vec{p}_i, s_i)$ returns the element of $\vec{p}_i$ that corresponds to user device s_i. Based on this loss function, the weights of mLSTM 2 are updated by: $\mathbf{W}_{\mathrm{d}} \leftarrow \mathbf{W}_{\mathrm{d}} - \mu_{\mathrm{d}}\frac{\partial \mathcal{L}_{\mathrm{d}}}{\partial \mathbf{W}_{\mathrm{d}}}$, where μ_{d} is the update step size ($\mu_{\mathrm{d}} = 0.01$ in our experiments).

The training of CNN has two purposes: i) minimizing the prediction loss $\mathcal{L}_{\mathrm{a}}$, and ii) maximizing the domain discrimination loss $\mathcal{L}_{\mathrm{d}}$. We define the combined loss function as follows: $\mathcal{L}_{\mathrm{e}} = \gamma\mathcal{L}_{\mathrm{a}} - \mathcal{L}_{\mathrm{d}}$, where γ is a tuning parameter ($\gamma = 0.2$ in our experiments). Based on this loss function, the weights of CNN are updated by: $\mathbf{W}_{\mathrm{e}} \leftarrow \mathbf{W}_{\mathrm{e}} - \mu_{\mathrm{e}}\frac{\partial \mathcal{L}_{\mathrm{e}}}{\partial \mathbf{W}_{\mathrm{e}}}$, where μ_{e} is the update step size ($\mu_{\mathrm{e}} = 0.01$ in our experiments). As a feature extractor, the CNN tries to cheat the user discriminator by maximizing its loss function $\mathcal{L}_{\mathrm{d}}$ while improving the performance of beam prediction by minimizing the loss function $\mathcal{L}_{\mathrm{a}}$. With this adversarial learning structure, TBP tends to extract the user-independent features for the beam prediction.

D. Prediction with Local Beam Search

After the model is trained, it then can be used for beam prediction based on the past beam samples in the database. In the inference phase, the predicted beam angles (the output of mLSTM 1) may or may not be accurate enough for packet transmission. Hence, TBP performs a *local* beam search, with the aim of finding the best beam angle for signal steering. Suppose that a mmWave device has a set of pre-defined beam azimuth angles $\{\alpha_p : 1 \le p \le N_p\}$ and a set of pre-defined beam elevation angles $\{\beta_q : 1 \le q \le N_q\}$. Also, recall that $(\hat{\alpha}, \hat{\beta})$ are prediction results of our model, i.e., the output of mLSTM 1 in Fig. 3. Then, the task of beam refinement module can be formulated as: $(p^*, q^*) = \arg\max_{p,q} f(\alpha_p, \beta_q)$, subject to $|\alpha_p - \hat{\alpha}| \le \tau_\alpha$ and $|\beta_q - \hat{\beta}| \le \tau_\beta$, where τ_α and τ_β are the thresholds for azimuth and elevation angles, respectively. $f(\alpha_p, \beta_q)$ is the resulting signal strength at receiver when the transmitter uses (α_p, β_q) as the azimuth/elevation beam angles. To find the optimal beam direction, we can perform the beam probing protocols in Section II-A. Since TBP only needs to perform a local search, its airtime overhead of beam training is much less than that of existing beam training schemes.

IV. TBP: Out-of-Band Enhancement

MmWave communication systems feature high bandwidth, small coverage, and susceptibility to blockage. Thus, it is expected that mmWave communication systems will coexist with sub-6GHz WiFi systems as they complement each other. In this section, we consider an indoor wireless communication network where each device is equipped with both mmWave and sub-6GHz WiFi radios. We aim to take advantage of widely-available sub-6GHz WiFi CSI to enhance the beam prediction for mmWave radio. This design is particularly useful for the case where mmWave radio is in the sparsity of past data samples for beam prediction (e.g., mmWave radio just wakes up from sleep mode, mmWave radio is inactive for a long time). Although the literature has many works on out-of-band beamforming [2], [4], [3], [5], [27], [34], their focus is mainly on simplifying beam search in the spatial domain. Here, TBP focuses on the temporal prediction of beam angles.

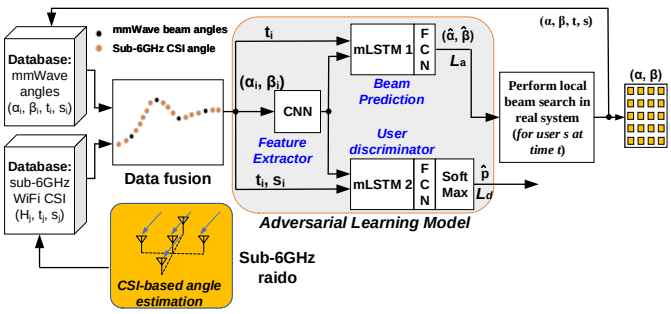

Fig. 6: The structure for TBP when taking into account sub-6GHz CSI for beam angle prediction.

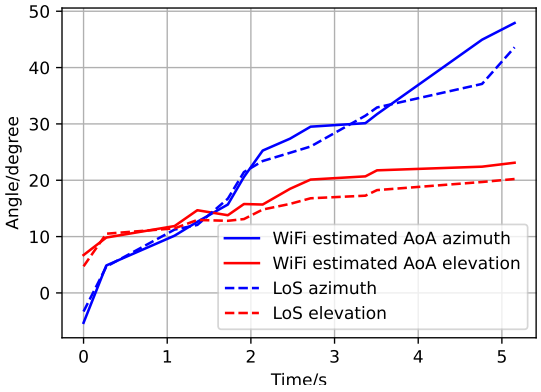

Fig. 7: The continuous angle-of-arrival (AoA) estimation from WiFi band and ground truth measured by laser meter.

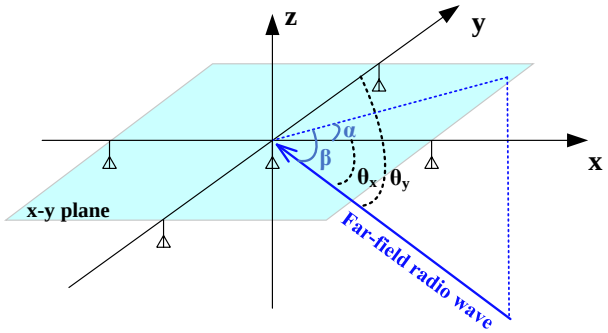

Fig. 8: Illustrating signal angles α, β, θ_{x}, and θ_{y} in 3D space.

A. Design

Fig. 6 shows the overall structure of TBP for the case when sub-6GHz CSI is available for beam prediction. Compared to the learning model in Fig. 3, the only difference is that it adds data from sub-6GHz radio for its training and inference. As shown in Fig. 6, the data sample from mmWave radio is denoted as $(\alpha_i, \beta_i, t_i, s_i)$, while the data sample from sub-6GHz radio is denoted as $(\mathbf{H}_j, t_j, s_i)$. Apparently, the data samples from the two radios are in very different formats.

An important question is how to combine the data from the two radios for training and inference. For this question, a straightforward method is concatenation, i.e., feeding all raw data to the CNN and letting the CNN extract the useful features. However, this method did not perform well in our experiments. We guess the reason is that the CNN is incapable of extracting meaningful features from the heterogeneous data samples. To address this problem, we could unify the data format from the two sources by converting the sub-6GHz CSI to the azimuth and elevation angles of the LoS path (see Fig. 7 for example), and then combine the best beam azimuth/elevation angles and the LoS azimuth/elevation angles as the input of CNN. While this method performs better than the previous method, its performance still remains unsatisfactory in our experiments.

It could be attributed to two reasons. The first one lies in the fact that the best-beam direction may differ from the LoS direction. Through a careful study of the CNN model's input and output data, we found that in a large portion of input data, there is a discrepancy between the LoS direction (calculated from sub-6GHz CSI) and the best-beam direction (obtained from mmWave search). This is not surprising. In practice, the best-beam direction deviates from the LoS direction due to the imperfect radiation pattern of patch antennas in mmWave systems and the presence of strong Non-LoS paths. The second reason is that CNN may not be capable of differentiating the best-beam direction from the LoS direction during training and inference. Due to the discrepancy between LoS and best-beam directions within the training data, the model faces challenges in distinguishing the best-beam direction from the LoS direction in the inference phase. This is because the direct-merging method depends solely on time alignment, without utilizing the best-beam direction obtained through mmWave search to correct the corresponding sub-6GHz LoS direction. Furthermore, the larger amount of sub-6GHz CSI data significantly diminishes the impact of the best-beam data generated from the mmWave search.

Based on the above observations, we propose a new method to convert sub-6GHz CSI to its azimuth and elevation angles. It comprises two steps: i) convert CSI to LoS azimuth/elevation angles, and ii) estimate the corresponding best-beam azimuth/elevation angles based on the LoS azimuth/elevation angles. The details are presented in the next subsection. After merging the data from the two radios, the system model is trained and operated in the same way as presented in Section III.

B. Data Fusion

We consider the case where the sub-6GHz radio is co-located with mmWave radio. We assume that sub-6GHz radio is equipped with multiple equally-spaced antenna elements along both x and y axes as illustrated in Fig. 8. To unify the data format for training and inference, we convert the sub-6GHz CSI data (i.e., $(\mathbf{H}_i, t_i)$) to corresponding azimuth/elevation angles (i.e., (α_i, β_i, t_i)). Fig. 9 shows the diagram of our data conversion method. It comprises two steps:

- *Step 1: Identifying anchor data samples.* In this step, we find those sub-6GHz CSI data samples that coincide with a mmWave data sample in time. In Fig. 9, CSI data $(\mathbf{H}_i, t_i)$ and $(\mathbf{H}_{i'}, t_{i'})$ are two examples showing the coincidence. Then, the corresponding azimuth/elevation angles of these two samples can be found, as shown in the

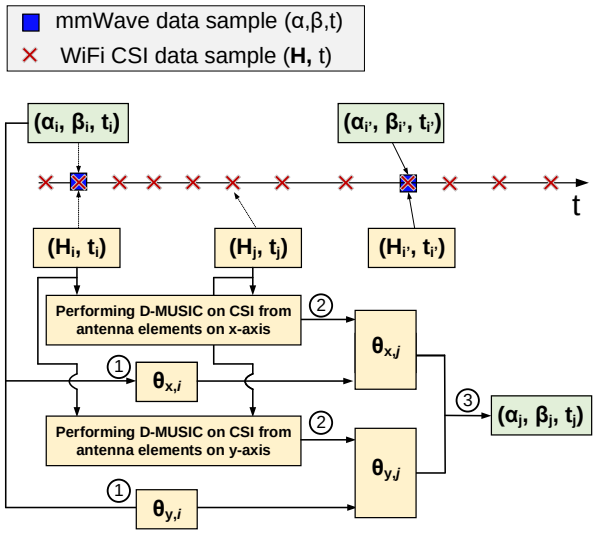

Fig. 9: The diagram of data fusion.

figure. These CSI data samples will be used as anchors to calculate the azimuth/elevation angles for the rest of CSI data samples. In practice, as long as the time gap between the CSI data sample and mmWave sample is less than 1 ms, we consider them in coincidence.

- *Step 2: Converting the resting CSI data samples.* The data conversion process is illustrated through the example of $(\mathbf{H}_j, t_j)$ in Fig. 9. We explain this process by the following three steps.

① Calculate $(\theta_{\mathrm{x},i}, \theta_{\mathrm{y},i})$ for Reference Data Sample. Consider an incoming signal in the 3D space as shown in Fig. 8. $\theta_{\mathrm{x},i}$ is the angle-of-arrival (AoA) of incoming signal for the linear antenna array on x-axis, while $\theta_{\mathrm{y},i}$ is the AoA of incoming signal for the linear antenna array on y-axis. Then, the relation between azimuth/elevation angles (α_i, β_i) and signal AoA $(\theta_{\mathrm{x},i}, \theta_{\mathrm{y},i})$ can be expressed as:

$$\theta_{\mathrm{x},i} = \cos^{-1}(\cos(\alpha_i)\cos(\beta_i)), \tag{2}$$

$$\theta_{\mathrm{y},i} = \cos^{-1}(\sin(\alpha_i)\cos(\beta_i)). \tag{3}$$

② Calculate $(\theta_{\mathrm{x},j}, \theta_{\mathrm{y},j})$ for Data Sample j. We first focus on the calculation of $\theta_{\mathrm{x},j}$ using the antenna elements on x axis as shown in Fig. 8. The calculation of $\theta_{\mathrm{y},j}$ will follow the same token using the antenna elements on y axis. Consider antenna k on x axis. The additional phase shift of its received signal with respect to the first antenna can be written as:

$$\phi_{\mathrm{x},k} = 2\pi\frac{(k-1)d}{\lambda}\cos(\theta_{\mathrm{x}}), \tag{4}$$

where λ is the wavelength, d is the antenna spacing, θ_{x} is the AoA of incoming signal.

Denote $\phi_{\mathrm{x},k,i}$ and $\phi_{\mathrm{x},k,j}$ are the additional phase shift on antenna k at time t_i and t_j, respectively. Then, we have

$$\phi_{\mathrm{x},k,j} - \phi_{\mathrm{x},k,i} = 2\pi\frac{(k-1)d}{\lambda}\left(\cos(\theta_{\mathrm{x},j}) - \cos(\theta_{\mathrm{x},i})\right). \tag{5}$$

Based on (5), we further have

$$\cos(\theta_{\mathrm{x},j}) - \cos(\theta_{\mathrm{x},i}) = \frac{\lambda}{2\pi(k-1)d}\cdot(\phi_{\mathrm{x},k,j} - \phi_{\mathrm{x},k,i}). \tag{6}$$

Denote $\mathbf{H}_{\mathrm{x},j} = [H_{\mathrm{x},1,j},\ H_{\mathrm{x},2,j},\ \cdots, H_{\mathrm{x},K,j}]$ as the channel vector measured on the antenna elements on x axis at time t_j. In (6), $\phi_{\mathrm{x},k,j}$ is a component of the phase of channel coefficient $H_{\mathrm{x},k,j}$; and $\phi_{\mathrm{x},k,i}$ is a component of the phase of channel coefficient $H_{\mathrm{x},k,i}$. It can be seen that the estimation problem in (6) is similar to the classic AoA estimation problem. Therefore, the left-hand side of (6) can be estimated using MUSIC algorithm with the input of $\mathbf{H}_{\mathrm{x},j}\odot(\mathbf{H}_{\mathrm{x},i})^*$, where $\odot$ is element-wise product and $(\cdot)^*$ is conjugate operator. Mathematically, we have

$$\cos(\theta_{\mathrm{x},j}) - \cos(\theta_{\mathrm{x},i}) = \mathrm{MUSIC}\left(\mathbf{H}_{\mathrm{x},j}\odot(\mathbf{H}_{\mathrm{x},i})^*\right), \tag{7}$$

where $\mathbf{H}_{\mathrm{x},j}$ and $\mathbf{H}_{\mathrm{x},i}$ are measured channels from the antenna elements on x axis at time t_j and t_i, respectively.

Based on (7), we have

$$\cos(\theta_{\mathrm{x},j}) = \cos(\theta_{\mathrm{x},i}) + \mathrm{MUSIC}\left(\mathbf{H}_{\mathrm{x},j}, \mathbf{H}_{\mathrm{x},i}\right), \tag{8}$$

By the same token, we have

$$\cos(\theta_{\mathrm{y},j}) = \cos(\theta_{\mathrm{y},i}) + \mathrm{MUSIC}\left(\mathbf{H}_{\mathrm{y},j}, \mathbf{H}_{\mathrm{y},i}\right). \tag{9}$$

③ Calculate (α_j, β_j, t_j) for Data Sample j. Given $\cos(\theta_{\mathrm{x},j})$ in (8) and $\cos(\theta_{\mathrm{y},j})$ in (9), we can calculate the desired (α_j, β_j) as follows:

$$\alpha_j = \tan^{-1}\left(\frac{\cos(\theta_{\mathrm{y},j})}{\cos(\theta_{\mathrm{x},j})}\right), \tag{10}$$

$$\beta_j = \cos^{-1}\left(\frac{\cos(\theta_{\mathrm{x},j})}{\cos(\alpha_j)}\right). \tag{11}$$

This completes the conversion from $(\mathbf{H}_j, t_j)$ to (α_j, β_j, t_j).

C. Training and Inference

The only purpose of out-of-band CSI from sub-6GHz radio is to enrich the dataset for the temporal mmWave beam prediction. It does not alter the training and inference procedure of TBP. That said, the training and inference operations in this case are the same as those in Section III.

V. Performance Evaluation

A. Implementation

60GHz mmWave Testbed. We built a mmWave testbed for the evaluation of TBP using EK1HMC6350 RF front-ends from Analog Devices. Fig. 10 shows the overall diagram of our testbed; and Fig. 11 shows a picture of the mmWave board. HMC6300 supports carrier frequency from 57GHz to 64GHz, and the bandwidth of each channel is 1.8GHz. Two planar antennas, each with 4×8 patch elements, are used for this testbed. One is for the transmitter, and the other is for the receiver. Since the planar antennas cannot steer its beam electronically; two stepper motors are installed to control the beam direction in the 3D space. One stepper motor controls the beam's azimuth angle; the other controls the beam's elevation angle. The angle resolution of stepper motors is 1.8 degree. The two stepper motors are controlled by the host computer via its USB interface. The mmWave radio RF front-end is connected to USRP X310 through baseband I/Q differential

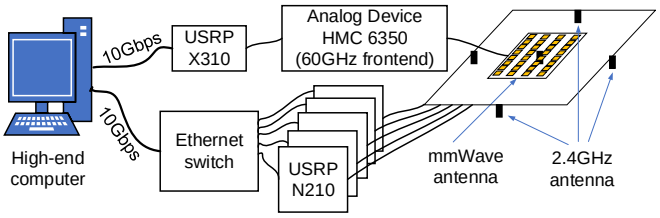

Fig. 10: Our testbed installed on the ceiling of a lab.

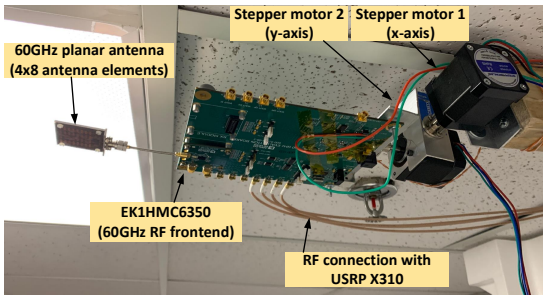

Fig. 11: The testbed installed on the ceiling of a lab.

interface, and USRP X310 is then connected to a high-performance computer through 10Gbps SFP+ cable. In our experiments, USRP X310 is installed with BasicTx and BasicRx daughter-boards to generate baseband signals. All signal processing modules were implemented in the host computer to measure the signal strength at receiver. Overall, the mmWave testbed can support 100MHz instantaneous bandwidth for real-time communication and 2-dimensional beam steering.

Sub-6GHz Radio for CSI Acquisition. As shown in Fig. 10, a 5-antenna SDR receiver was built using an array of synchronized USRP N210 devices to obtain the CSI for the evaluation of TBP when CSI is taken into account. The 5 omnidirectional antennas are deployed in a cross shape with 3 antennas on x axis and 3 on y axis. The sub-6GHz system implements commodity 802.11 protocol with a bandwidth of 20MHz.

TBP Implementation. We implement TBP in the host computer as shown in Fig. 10 using TensorFlow [35]. The database records the past beam selection information, which will be used for the beam prediction over time. The data collection is automated using the beam angles from the local beam search module in Fig. 3.

B. Experimental Settings

Our experiments were conducted in four scenarios: a lab, a conference room, a hallway and an apartment. The lab is 220 ft^2, with typical cubicles and furniture. The conference room is about 170 ft^2, with a big table and multiple chairs. The hallway is relatively large and empty with a few display cases near the wall. The apartment is about 260 ft^2, furnished with common items such as a tea table, chairs, sofa, and TV. In each scenario, the mmWave radio was installed on the ceiling, communicating with a mmWave device carried by six different persons on the floor.

In each scenario, six persons walked along their routing paths sequentially, and 1,920 trace samples were collected in total. 30% of the trace data are randomly selected and used for testing purposes. Along the routing path, the beam angle samples are recorded in irregular time intervals varying from tens to hundreds of milliseconds, and sub-6GHz Wi-Fi CSI was measured once per millisecond.

C. Training Process

The model was trained in each individual scenario. Fig. 12 presents the training and test loss in the lab scenario across various cases. Examining the training loss for a single-user case in Fig. 12a, we observed that the model converges after approximately 60 epochs. When combining mmWave data with out-of-band CSI, we observed that the convergence time extends to 80 epochs, as depicted in Fig. 12b. This can be attributed to the increased complexity of the data. Comparing the cases with and without out-of-band CSI, we observed that the loss decreases more rapidly at the beginning of training when incorporating the out-of-band CSI. This suggests that the beam direction pattern becomes more discernible with the additional information. Fig. 12c shows the training loss for the multi-user case, taking around 100 epochs for the model to converge due to the high complexity of multi-user data.

D. Performance Metrics and Comparison Baseline

Metrics. We use the prediction error as the performance metric. Specifically, referring to Fig. 3, the prediction error of azimuth angle is $e_\alpha = |\alpha - \hat{\alpha}|$, where $\hat{\alpha}$ is the predicted beam azimuth angle while α is the beam angle after beam refinement. Similarly, the prediction error of elevation angle is $e_\beta = |\beta - \hat{\beta}|$.

Comparison Baselines. Two schemes are used as the comparison baselines for the evaluation of TBP.

- *Previous Azimuth/Elevation Angle:* For this scheme, we simply use the previous beam's azimuth/elevation angle as the beam direction for the current packet transmission. Apparently, the performance of this scheme is highly dependent on the mmWave data sampling rate and the movement speed of the target mmWave device as well as the dynamics of the environment.
- *LSTM Model:* This scheme uses a traditional LSTM model to predict the beam angles based on the history of beam angle information. Specifically, we replace the mLSTM in Fig. 3 with a traditional LSTM for the beam prediction and remove the adversarial learning components.

E. Experimental Results: Beam Angle Errors

In this subsection, we measure the performance of TBP. In addition, we explore the answers to the following questions: For a mmWave AP, is it necessary to create and train a model for each individual user device? If a mmWave AP maintains a separately trained model for each individual user device, would it offer a better performance than the case where the mmWave AP uses a single model for all user devices? To seek the answers, we conduct experiments in two cases: single-user case and multi-user case, as detailed below.

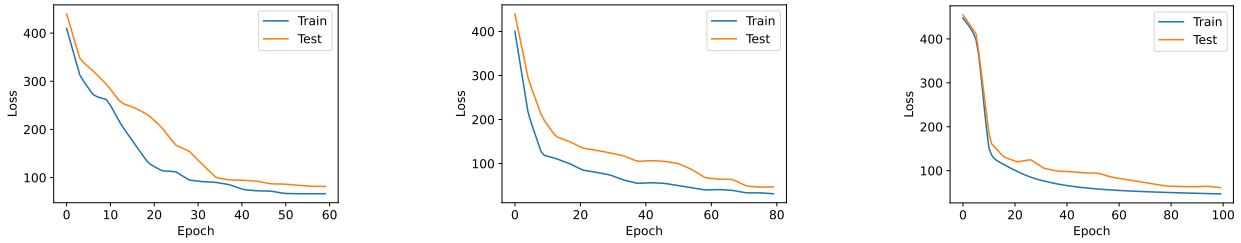

(a) Single-user case. (b) Single-user with out-of-band CSI. (c) Multi-user case.

Fig. 12: Training and test loss for TBP in lab scenario.

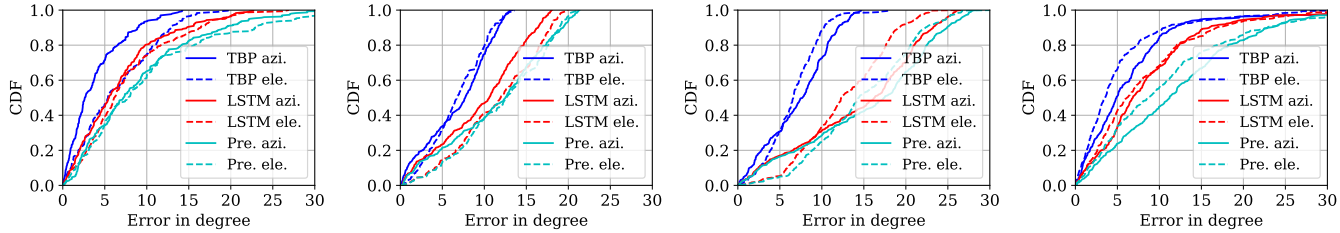

(a) Lab scenario. (b) Conference room scenario. (c) Hallway scenario. (d) Apartment scenario.

Fig. 13: Prediction error for TBP: single-user case.

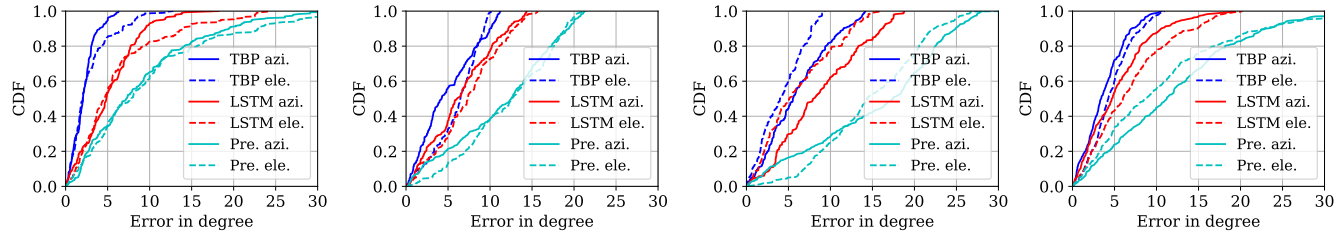

(a) Lab scenario. (b) Conference room scenario. (c) Hallway scenario. (d) Apartment scenario.

Fig. 14: Prediction error for TBP: Single-user case with out-of-band CSI enhancement.

TABLE I: Prediction errors of TBP: single-user case.

	TBP's prediction error (degree)								LSTM's prediction error (degree)								Previous Point's prediction error (degree)			
	w/o CSI				w/ CSI				w/o CSI				w/ CSI				–			
	Avg		95%		Avg		95%		Avg		95%		Avg		95%		Avg		95%	
	azi	ele	azi	ele	azi	ele	azi	ele	azi	ele	azi	ele	azi	ele	azi	ele	azi	ele	azi	ele
lab	3.8	6.3	11.2	14.7	2.1	2.8	5.0	8.2	6.7	7.5	18.8	19.3	5.2	6.2	11.6	18.6	8.9	9.8	22.2	27.8
conference	6.9	6.8	12.2	12.1	4.9	6.1	10.7	9.6	9.6	11.4	17.0	18.7	6.5	7.3	13.6	14.0	11.3	12.1	20.1	19.8
hallway	7.1	6.6	13.3	11.4	6.0	4.1	12.8	8.7	14.3	12.7	24.8	21.3	8.7	6.1	17.3	13.9	15.3	14.8	26.5	24.8
apartment	6.5	5.0	15.6	16.8	3.8	4.5	8.5	9.3	8.6	8.1	21.1	23.1	5.3	6.8	13.3	16.2	12.4	10.6	27.3	27.5

Single-User Case. We first evaluate the performance of TBP based on the history beam selection profile (without CSI from sub-6GHz radio).

Fig. 13 shows the CDF of the prediction errors in four scenarios, and Table I summarizes their average and 95-percentile prediction errors. It can be seen that TBP performs better than the other two schemes. In most cases, the average prediction error of TBP is less than 7 degrees, and the 95-percentile of its prediction error is less than 16 degrees. Both of them are smaller than the other two schemes. Particularly, TBP significantly outperforms the LSTM-based scheme. This indicates that our proposed mLSTM structure is much more efficient for beam angle prediction than the traditional LSTM structure.

We now report the experimental results of TBP when it takes advantage of available CSI data from co-located sub-6GHz radio for its training and inference. Fig. 14 shows the CDF of the measured prediction errors, and Table I shows the comparison between the cases with and without CSI data from sub-6GHz radio. It can be seen that, with the utilization of CSI from sub-6GHz radio, the average prediction error of TBP is less than 3 degrees in the lab scenario. The average prediction error is around 5 degrees in the conference room, hallway, and apartment scenarios. It is larger than that in the lab scenario mainly because of their large size. It can also be seen that the use of CSI data can notably improve the prediction accuracy in the lab scenario and slightly improve the prediction accuracy in the conference room, hallway and apartment scenarios. This

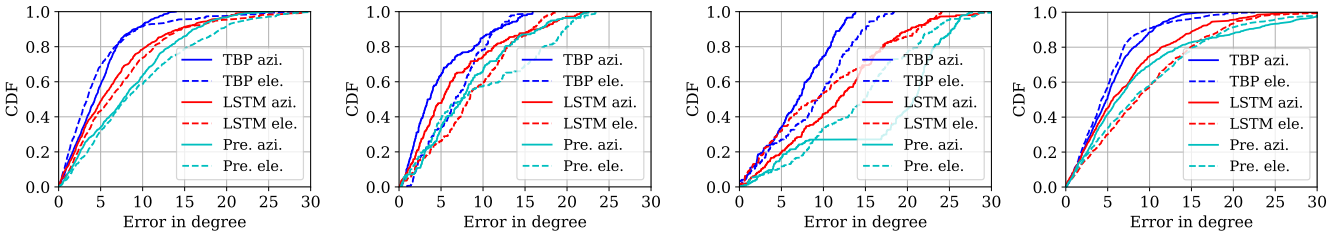

(a) Lab scenario. (b) Conference room scenario. (c) Hallway scenario. (d) Apartment scenario.

Fig. 15: Prediction error for TBP: multi-user case.

TABLE II: Prediction errors for TBP: multi-user case.

scenario	TBP's prediction error (degree)				LSTM's prediction error (degree)				Previous Point's prediction error (degree)			
	Avg		95%		Avg		95%		Avg		95%	
	azi	ele	azi	ele	azi	ele	azi	ele	azi	ele	azi	ele
lab	4.9	4.8	10.9	13.8	6.5	7.3	18.0	19.1	8.3	9.5	18.3	22.4
conference	5.1	6.8	14.1	13.1	6.8	8.6	18.9	16.9	8.3	9.6	18.5	20.8
hallway	6.9	8.7	12.6	16.2	11.6	10.1	22.5	22.7	17.1	14.1	26.2	24.7
apartment	5.3	5.0	12.1	13.2	7.2	9.3	19.1	20.6	8.7	9.6	27.1	24.2

is because the lab has many furniture and equipment and thus is more reflective than the other three scenarios.

Multi-User Case. We conduct experiments in the four scenarios by creating and training a single TBP model for six user devices, and measure the prediction errors to evaluate its performance. Fig. 15 presents the CDF of our measured prediction errors in the four scenarios, and Table II summarizes the average and 95th percentile of the measured prediction errors. It can be seen that, for most cases, the average prediction error of TBP is less than 7 degrees. In addition, TBP significantly outperforms its counterparts (LSTM-based scheme and previous beam scheme). Compared to the results presented in Table I and Table II, we found that TBP has similar performance in the single-user and multi-user cases. This indicates that a mmWave AP does not need to maintain (create, train, and re-train) different TBP models for different user devices. In other words, it only needs to maintain a single TBP model for all user devices.

F. Throughput Gain

Based on the measured beam angle prediction errors, we now assess the throughput gain of TBP in some representative scenarios.

Comparison Baseline. We use the beam search approach in IEEE 802.11ad (see Section II-A) as our comparison baseline.[1] Following the beam search parameters in [2], we assume that the beam search range is from 0° to 180°, with the step size being 7°. Also following the setting in [2], we assume that the measurement of one beam direction takes 60 μs. Therefore, to search for the best azimuth and elevation angles in the 3D space, it takes about $\frac{180}{7} \times \frac{180}{7} \times 60\ \mu\text{s} = 39.6$ ms. This is the airtime overhead of beam search during a beacon interval in conventional mmWave networks.

[1]One may wonder why we use IEEE 802.11ad beam search (rather than the more advanced beam search schemes in the literature) as our comparison baseline. We argue that, while there are many efficient beam search schemes in the literature [2], [7], [12], [13], [3], most of them are limited to the spatial domain. TBP is the first temporal beam prediction approach and complementary to those schemes. Simply put, TBP can be used on top of those beam search schemes to further improve the throughput of mmWave networks.

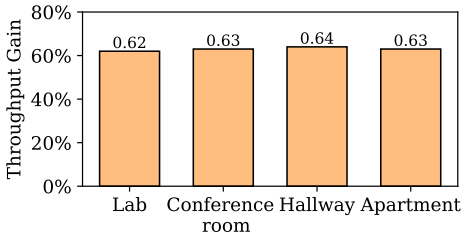

Fig. 16: Throughput gain of TBP over the 802.11ad beam search approach based on the measured beam prediction errors.

To evaluate the throughput, another important factor is the time duration of a beacon interval (see Fig. 2). Theoretically, a longer beacon interval will improve the throughput by amortizing the beam search overhead. However, in practice, the maximum time duration of a beacon interval is constrained by channel coherence time. Here, we follow the parameters in [36] by setting the beacon interval to 100 ms.

Throughput Gain. When a mmWave device uses TBP, it does not need to search for the whole angle range (i.e., 0° to 180°). It only needs to refine the beam direction within its prediction error range. Consider TBP in the lab scenario for example. Its 99-percentile prediction error is 13.0 degrees for azimuth angle and 24.4 degrees for elevation angle. Therefore, the beam search time can be estimated by $\frac{13\times2}{7} \times \frac{24.4\times2}{7} \times 60\ \mu\text{s} = 1.55$ ms, where 7 is the angle search step size and 60 μs is the airtime of one search. Recall that we assume the beacon interval is 100 ms. Then, TBP has $100 - 1.55 = 98.45$ ms for data transmission. In contrast, the conventional beam search approach (comparison baseline) has $100 - 39.6 = 60.4$ ms for data transmission. This means that TBP can improve the throughput by 62%. Following the same approach, we also calculate the throughput gain of TBP in other three scenarios. Fig. 16 presents the projected throughput gain of TBP. It can be observed that TBP improves the throughput by more than 60% in all four scenarios. This shows the efficiency and robustness of TBP in different environments.

VI. LIMITATIONS AND DISCUSSIONS

Evaluation and Testbed. In this work, we evaluated our design on a custom-made mmWave testbed. While we used the planar patch antennas for mmWave transmission and reception, their beam steering function was implemented using mechanic

stepper motors. As such, the beam pattern generated by this testbed may not be exactly the same as commercial mmWave communication devices. To address this limitation, our future work will focus on the implementation and evaluation of TBP on commercial mmWave devices. We plan to use Sivers EVK02004 (28GHz) [37] and EVK06003 (60GHz) [38] for our implementation and evaluation. Those devices support electric beamforming in real time.

Generalizability of LSTM Model. Despite the recent advancement of deep learning models, generalizability is still a fundamental challenge in many of their applications. The propagation of mmWave signals is highly dependent on the surroundings in a specific environment. Currently, TBP has limited generalizability capability. When used in a new environment, TBP needs to be fine-tuned using the data from that environment. This requirement undermines its applicability. In our future work, we will design a data collection tool to enable the automation of the fine-tuning of TBP.

VII. Related Work

We review prior works in the following categories.

Learning-based Beam Search. Pioneering works have been done to predict the beam direction using deep learning. [13], [14] studied the beamforming problem in highly-mobile mmWave systems. Their primary emphasis is on vehicular communications within outdoor scenarios featuring multiple base stations. They demonstrate the capability to predict the optimal beam by jointly analyzing the uplink signal received at these stations. However, it is noteworthy that the network traffic pattern for vehicular communications significantly differs from that of indoor scenarios. Vehicular environments involve high-speed mobility, but the trajectory dynamics are less pronounced compared to indoor scenarios. Consequently, these studies exclusively employ traditional deep neural networks without considering the time interval.

In the communication scenarios beyond vehicular contexts, [15] specifically targets indoor environments. This study takes into account the orientation of the user's device at each location, employing spatial features in 3D space to train the neural network and align the beam. DeepIA [16] trains a deep learning model to predict the best beam based on received signal strength (RSS) obtained from a subset of beams. However, this approach still necessitates scanning a subset of beams each time, resulting in a significant overhead for mobile millimeter networks. [17] is the most relevant work to our work. It proposed a deep learning-based beam tracking scheme for mobile mmWave devices. Unlike our work, which primarily relies on the user's moving trajectory to predict the optimal beam direction, this study focuses on estimating dynamic channels resulting from the user's minor motion. Additionally, it incorporates Inertial Measurement Unit (IMU) sensor measurements as additional input data. The works mentioned above do not consider practical issues such as non-uniform and non-smooth data samples, and they are evaluated through simulation. In contrast, TBP is a practical design and is evaluated via realistic experiments.

Deepbeam [18] is the only work that has been implemented on a testbed. It listens to the data transmission between the AP and other users, learning unique patterns from the in-phase-quadrature (I/Q) representation of the waveform. This allows it to predict the beam utilized by the transmitter and AoA on the receiver side. However, it relies heavily on other devices in the environment and primarily focuses on leveraging spatial features, a distinction from TBP. On the other hand, [39] improves this method by proposing a deep regularized waveform learning (DRWL) strategy. This approach demonstrates the ability to predict beams even with limited samples, showcasing advancements beyond its predecessor.

TABLE III: Out-of-Band beamforming for mmWave device.

Ref.	Out-of-Band	sensor or antenna array	2D/3D	Error range
BBS [2]	WiFi band	8 antennas	2D	4°
[4]	sub-6GHz	4 antennas	2D	10°
MUST [3]	WiFi band	3 antennas	3D	10°
[5]	sub-6GHz	8 antennas	2D	N/A
Listeer [27]	Light	light sensor array	3D	3.5°
[34]	Images	Camera	3D	N/A
TBP	WiFi band	5 antennas	3D	7°

The work by [40] focuses on beam tracking in UAV-mmWave communication, modeling the problem as a multi-variable Gaussian process and using the Gaussian Process Machine Learning (GPML) method to address it. However, it is noteworthy that UAVs typically follow a pre-defined path with an existing LoS path for communication, distinguishing it from our approach.

Out-of-Band Assistance for Beam Search. Our work is also related to the research in this area. Table III compares our work with prior works. The works [2], [4], [3], [5] harness the WiFi band to infer the beam directions for mmWave communications. Most of them use linear antenna arrays for beam search and are limited to the beam search in a 2D plane. MUST [3] studied the beam search in 3D space using an array of three antennas. It achieves 71.2% prediction accuracy and 10° beam tracking error. [41] proposes a self-supervised deep learning approach, directly mapping the CSI from sub-6GHz to mmWave beams. TBP was inspired by these works but uses the out-of-band CSI in a different way. It converts the sub-6GHz CSI information to the best-beam azimuth and elevation angles based on history sub-6GHz CSI and mmWave beam angles.

Besides leveraging out-of-band information from the radio side, LiSteer [27] determines the mmWave beamforming direction by tracking indicator LEDs on APs. Since it relies on light resources, LoS is required for this solution. Taking a further step, [34] inputs images captured by the transmitter and receiver into a deep neural network, identifying beam directions based on these images. However, both of these methods require an additional sensor installation on the AP, which may not be suited for practical mmWave systems.

Compressive Sensing. In addition to out-of-band beamforming, compressive sensing technique has been studied for mmWave beamforming in order to reduce the beam search overhead [6], [7]. In [6], compressive sensing is directly applied for beamforming. But it relies on the accurate phase measurement. In practice, accurate phase information may not be available due to the existence of carrier frequency offset. Agile-Link [7] hashes the beam directions and utilizes a voting

mechanism to recover the directions. It can identify the best path by tracking the change of energy across different bins in a logarithmic number of measurements. The works in this area focus on exploiting the spatial correlation of wireless channels to facilitate the beam search. In contrast, TBP exploits the temporal channel correlation for beam prediction.

Hierarchical Beam Search. To accelerate the beam search process, some works have formulated the beam search problem as an optimization problem [9], [10], [11]. Sophisticated algorithms have been developed to search the possible beams in a hierarchical manner so as to minimize the search time. In practice, the signals from different paths may cancel each other, leading to an inaccurate estimation of the power in the beam search process. However, these works are all based on simulation and without considering practical issues such as non-ideal antenna radiation and multipath effect. Clearly, TBP differs from this research line.

Model-based Beam Forecast. [26] studied model-based beam forecast by utilizing the spatial correlation of 60GHz near-field channels to predict the future channel when Tx/Rx moves. It relies on the anchor point channel profile to reconstruct the channel profiles for nearby points. However, when a user moves too far from the anchor point, the beam scanning will still be triggered.

VIII. CONCLUSION

Analog beamforming is a fundamental problem in mmWave communication systems. One key problem related to analog beamforming is how to reduce the airtime overhead of beam selection as it is critical for improving the efficiency of mmWave communications. In this paper, we presented TBP for beam prediction in a 3D space by leveraging the temporal correlation of mmWave channels. The innovation of TBP lies in the design of a new LSTM model, which is capable of performing accurate beam prediction by taking non-uniform, non-smooth history data samples. We further enhanced TBP by taking out-of-band CSI from sub-6GHz radio as its input for training and inference. A novel data fusion method was developed to unify the format of the data samples from the mmWave and sub-6GHz radios. We have evaluated the performance of TBP on a 60GHz mmWave testbed. Experimental results show that the average prediction error of TBP is less than 7 degrees in most of our tested cases and that TBP can improve the throughput by more than 60% in representative mmWave networks.

Our future work will focus on three directions. First, we will develop a high-fidelity testbed for the evaluation of TBP. We will evaluate it on both 28GHz and 60GHz mmWave testbeds following the 5G/WiFi standards. Second, we are currently using the LSTM model for the beam prediction. More advanced deep-learning models have been developed for computer vision and natural language processing. We will enhance TBP by employing new models and evaluating their performance in real-world systems. Third, we will design tools and protocols to enable the automation of data collection for the model training of TBP. Such tools will significantly improve the practicality and generalizability of TBP.

REFERENCES

[1] W. Roh, J.-Y. Seol, J. Park, B. Lee, J. Lee, Y. Kim, J. Cho, K. Cheun, and F. Aryanfar, "Millimeter-wave beamforming as an enabling technology for 5G cellular communications: Theoretical feasibility and prototype results," *IEEE Communications Magazine*, vol. 52, no. 2, pp. 106–113, 2014.

[2] T. Nitsche, A. B. Flores, E. W. Knightly, and J. Widmer, "Steering with eyes closed: mm-wave beam steering without in-band measurement," in *Proceedings of IEEE Conference on Computer Communications (INFOCOM)*, pp. 2416–2424, IEEE, 2015.

[3] S. Sur, I. Pefkianakis, X. Zhang, and K.-H. Kim, "WiFi-assisted 60 GHz wireless networks," in *Proceedings of the 23rd Annual International Conference on Mobile Computing and Networking*, pp. 28–41, 2017.

[4] M. Hashemi, C. E. Koksal, and N. B. Shroff, "Out-of-band millimeter wave beamforming and communications to achieve low latency and high energy efficiency in 5G systems," *IEEE Transactions on Communications*, vol. 66, no. 2, pp. 875–888, 2017.

[5] A. Ali, N. González-Prelcic, and R. W. Heath, "Millimeter wave beam-selection using out-of-band spatial information," *IEEE Transactions on Wireless Communications*, vol. 17, no. 2, pp. 1038–1052, 2017.

[6] D. Ramasamy, S. Venkateswaran, and U. Madhow, "Compressive tracking with 1000-element arrays: A framework for multi-Gbps mmWave cellular downlinks," in *Proceedings of 50th Annual Allerton Conference on Communication, Control, and Computing (Allerton)*, pp. 690–697, IEEE, 2012.

[7] H. Hassanieh, O. Abari, M. Rodriguez, M. Abdelghany, D. Katabi, and P. Indyk, "Fast millimeter wave beam alignment," in *Proceedings of the 2018 Conference of the ACM Special Interest Group on Data Communication*, pp. 432–445, 2018.

[8] M. E. Rasekh, Z. Marzi, Y. Zhu, U. Madhow, and H. Zheng, "Noncoherent mmwave path tracking," in *Proceedings of the 18th International Workshop on Mobile Computing Systems and Applications*, pp. 13–18, 2017.

[9] W. Yuan, S. M. Armour, and A. Doufexi, "An efficient and low-complexity beam training technique for mmwave communication," in *2015 IEEE 26th Annual International Symposium on Personal, Indoor, and Mobile Radio Communications (PIMRC)*, pp. 303–308, IEEE, 2015.

[10] B. Li, Z. Zhou, W. Zou, X. Sun, and G. Du, "On the efficient beamforming training for 60ghz wireless personal area networks," *IEEE Transactions on Wireless Communications*, vol. 12, no. 2, pp. 504–515, 2012.

[11] Y. M. Tsang, A. S. Poon, and S. Addepalli, "Coding the beams: Improving beamforming training in mmwave communication system," in *Proceedings of IEEE Global Telecommunications Conference-GLOBECOM 2011*, pp. 1–6, IEEE, 2011.

[12] A. Alkhateeb, O. El Ayach, G. Leus, and R. W. Heath, "Channel estimation and hybrid precoding for millimeter wave cellular systems," *IEEE Journal of Selected Topics in Signal Processing*, vol. 8, no. 5, pp. 831–846, 2014.

[13] A. Alkhateeb, S. Alex, P. Varkey, Y. Li, Q. Qu, and D. Tujkovic, "Deep learning coordinated beamforming for highly-mobile millimeter wave systems," *IEEE Access*, vol. 6, pp. 37328–37348, 2018.

[14] Y. Guo, Z. Wang, M. Li, and Q. Liu, "Machine learning based mmwave channel tracking in vehicular scenario," in *Proceedings of IEEE International Conference on Communications Workshops (ICC Workshops)*, pp. 1–6, IEEE, 2019.

[15] S. Rezaie, E. De Carvalho, and C. N. Manchón, "A deep learning approach to location-and orientation-aided 3d beam selection for mmwave communications," *IEEE Transactions on Wireless Communications*, vol. 21, no. 12, pp. 11110–11124, 2022.

[16] T. S. Cousik, V. K. Shah, T. Erpek, Y. E. Sagduyu, and J. H. Reed, "Deep learning for fast and reliable initial access in ai-driven 6g mm wave networks," *IEEE Transactions on Network Science and Engineering*, 2022.

[17] S. H. Lim, S. Kim, B. Shim, and J. W. Choi, "Deep learning-based beam tracking for millimeter-wave communications under mobility," *IEEE Transactions on Communications*, vol. 69, no. 11, pp. 7458–7469, 2021.

[18] M. Polese, F. Restuccia, and T. Melodia, "Deepbeam: Deep waveform learning for coordination-free beam management in mmwave networks," in *Proceedings of the Twenty-second International Symposium on Theory, Algorithmic Foundations, and Protocol Design for Mobile Networks and Mobile Computing*, pp. 61–70, 2021.

[19] A. Alahi, K. Goel, V. Ramanathan, A. Robicquet, L. Fei-Fei, and S. Savarese, "Social LSTM: Human trajectory prediction in crowded

spaces," in *Proceedings of the IEEE conference on computer vision and pattern recognition*, pp. 961–971, 2016.
[20] A. Gupta, J. Johnson, L. Fei-Fei, S. Savarese, and A. Alahi, "Social GAN: Socially acceptable trajectories with generative adversarial networks," in *Proceedings of the IEEE Conference on Computer Vision and Pattern Recognition*, pp. 2255–2264, 2018.
[21] H. Xue, D. Q. Huynh, and M. Reynolds, "SS-LSTM: A hierarchical LSTM model for pedestrian trajectory prediction," in *Proceedings of IEEE Winter Conference on Applications of Computer Vision (WACV)*, pp. 1186–1194, IEEE, 2018.
[22] S. Hochreiter and J. Schmidhuber, "Long short-term memory," *Neural computation*, vol. 9, no. 8, pp. 1735–1780, 1997.
[23] S. Shin and H. Schulzrinne, "Measurement and analysis of the voip capacity in ieee 802.11 wlan," *IEEE Transactions on Mobile Computing*, vol. 8, no. 9, pp. 1265–1279, 2009.
[24] "IEEE 802.11ad." https://www.ieee802.org/11/Reports/tgad_update.html, Accessed: 30-July-2022.
[25] S. Sur, I. Pefkianakis, X. Zhang, and K.-H. Kim, "Towards scalable and ubiquitous millimeter-wave wireless networks," in *Proceedings of the 24th Annual International Conference on Mobile Computing and Networking*, pp. 257–271, 2018.
[26] A. Zhou, X. Zhang, and H. Ma, "Beam-forecast: Facilitating mobile 60 ghz networks via model-driven beam steering," in *Proceedings of IEEE Conference on Computer Communications (INFOCOM)*, pp. 1–9, IEEE, 2017.
[27] M. K. Haider, Y. Ghasempour, D. Koutsonikolas, and E. W. Knightly, "Listeer: mmwave beam acquisition and steering by tracking indicator LEDs on wireless APs," in *Proceedings of the 24th Annual International Conference on Mobile Computing and Networking*, pp. 273–288, 2018.
[28] W. Jiang, C. Miao, F. Ma, S. Yao, Y. Wang, Y. Yuan, H. Xue, C. Song, X. Ma, D. Koutsonikolas, *et al.*, "Towards environment independent device free human activity recognition," in *Proceedings of the 24th Annual International Conference on Mobile Computing and Networking*, pp. 289–304, 2018.
[29] D. Neil, M. Pfeiffer, and S.-C. Liu, "Phased LSTM: Accelerating recurrent network training for long or event-based sequences," *arXiv preprint arXiv:1610.09513*, 2016.
[30] Z. C. Lipton, D. C. Kale, C. Elkan, and R. Wetzel, "Learning to diagnose with LSTM recurrent neural networks," *arXiv preprint arXiv:1511.03677*, 2015.
[31] I. M. Baytas, C. Xiao, X. Zhang, F. Wang, A. K. Jain, and J. Zhou, "Patient subtyping via time-aware LSTM networks," in *Proceedings of the 23rd ACM SIGKDD international conference on knowledge discovery and data mining*, pp. 65–74, 2017.
[32] "Release 15." https://www.3gpp.org/release-15, Accessed: 30-July-2022.
[33] M. Giordani, M. Polese, A. Roy, D. Castor, and M. Zorzi, "A tutorial on beam management for 3GPP NR at mmwave frequencies," *IEEE Communications Surveys & Tutorials*, vol. 21, no. 1, pp. 173–196, 2018.
[34] B. Salehi, M. Belgiovine, S. G. Sanchez, J. Dy, S. Ioannidis, and K. Chowdhury, "Machine learning on camera images for fast mmwave beamforming," in *IEEE 17th International Conference on Mobile Ad Hoc and Sensor Systems (MASS)*, pp. 338–346, IEEE, 2020.
[35] M. Abadi, P. Barham, J. Chen, Z. Chen, A. Davis, J. Dean, M. Devin, S. Ghemawat, G. Irving, M. Isard, *et al.*, "Tensorflow: A system for large-scale machine learning," in *Proceedings of 12th USENIX symposium on operating systems design and implementation (OSDI)*, pp. 265–283, 2016.
[36] T. Nitsche, C. Cordeiro, A. B. Flores, E. W. Knightly, E. Perahia, and J. C. Widmer, "Ieee 802.11 ad: directional 60 ghz communication for multi-gigabit-per-second wi-fi," *IEEE Communications Magazine*, vol. 52, no. 12, pp. 132–141, 2014.
[37] "Sivers Semiconductors EVK02004." http://tinyurl.com/mr2n56k8, Accessed: 22-December-2023.
[38] "Sivers Semiconductors EVK06003." http://tinyurl.com/yc8zuvah, Accessed: 22-December-2023.
[39] H. Huang, G. Gui, H. Gacanin, C. Yuen, H. Sari, and F. Adachi, "Deep regularized waveform learning for beam prediction with limited samples in non-cooperative mmwave systems," *IEEE Transactions on Vehicular Technology*, 2023.
[40] Y. Ke, H. Gao, W. Xu, L. Li, L. Guo, and Z. Feng, "Position prediction based fast beam tracking scheme for multi-user uav-mmwave communications," in *ICC 2019-2019 IEEE International Conference on Communications (ICC)*, pp. 1–7, IEEE, 2019.
[41] I. Chafaa, R. Negrel, E. V. Belmega, and M. Debbah, "Self-supervised deep learning for mmwave beam steering exploiting sub-6 ghz channels," *IEEE Transactions on Wireless Communications*, vol. 21, no. 10, pp. 8803–8816, 2022.

Shichen Zhang is currently a Ph.D. student in the Department of Computer Science and Engineering at Michigan State University (MSU), East Lansing, MI. He received his B.Eng. degree in Automation from Beijing University of Technology, Beijing, China, in 2018 and M.Eng. degree in Electrical and Computer Engineering from Cornell University, Ithaca, NY, in 2019. His current research interests focus on wireless networks, sensing systems, and deep learning.

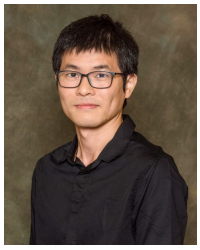

Qiben Yan (S'11–M'15–SM'21) is an Assistant Professor in Department of Computer Science and Engineering of Michigan State University. He received his Ph.D. in Computer Science department from Virginia Tech, an M.S. and a B.S. degree in Electronic Engineering from Fudan University in Shanghai, China. He is a recipient of NSF CRII award in 2016. His current research interests include cyber physical systems, wireless network security and privacy, mobile and IoT security, and big data privacy.

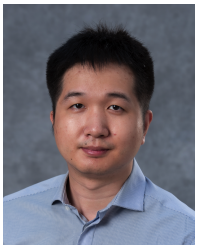

Tianxing Li is an Assistant Professor in the Computer Science and Engineering Department at Michigan State University (MSU). Prior to MSU, He was a Post-doc in the Computer Science Department at UMASS Amherst. He received his Ph.D. in the Computer Science Department at Dartmouth College in 2020. His research interests are in wireless communication, sensing, and low-power systems. He was the recipient of IEEE PerCom Best Paper Award in 2023, ACM SIGMOBILE Research Highlights in 2016, 2018, and 2021, and CACM Research Highlights in 2018.

Li Xiao (SM'10) received the B.S. and M.S. degrees in computer science from Northwestern Polytechnic University, China, and the Ph.D. degree in computer science from the College of William and Mary. She is a Professor of computer science and engineering with Michigan State University. Her research interests are in the areas of distributed and networking systems, overlay systems and applications, and wireless networks.

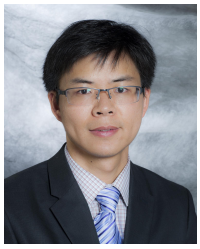

Huacheng Zeng (SM'20) received a Ph.D. degree in Computer Engineering from Virginia Polytechnic Institute and State University (Virginia Tech), Blacksburg, VA. He is currently an Assistant Professor in the Department of Computer Science and Engineering at Michigan State University (MSU), East Lansing, MI. Prior to joining MSU, he was an Assistant Professor of Electrical and Computer Engineering at the University of Louisville, Louisville, KY, and a Senior System Engineer at Marvell Semiconductor, Santa Clara, CA. He is a recipient of the NSF CAREER Award. He received the Best Paper Award from IEEE SECON 2021 and ACM WUWNet 2014. His research interest is broadly in wireless networking and sensing systems.